Title

Radical SAM-dependent formation of a nitrogenase cofactor core on NifB

Authors

Liu, Yiling A

Quechol, Robert

Solomon, Joseph B

et al.

Publication Date

2022-08-01

DOI

10.1016/j.jinorgbio.2022.111837

Peer reviewed

HHS Public Access

Author manuscript

J Inorg Biochem. Author manuscript; available in PMC 2023 August 01.

Published in final edited form as:

J Inorg Biochem. 2022 August ; 233: 111837. doi:10.1016/j.jinorgbio.2022.111837.

Radical SAM-dependent formation of a nitrogenase cofactor core on NifB

Yiling A. Liu[1,‖], **Robert Quechol**[1,‖], **Joseph B. Solomon**[1,2], **Chi Chung Lee**[1], **Markus W. Ribbe**[1,2,*], **Yilin Hu**[1,*], **Britt Hedman**[3,*], **Keith O. Hodgson**[3,4,*]

[1]Department of Molecular Biology and Biochemistry, University of California, Irvine, California 92697-3900.

[2]Department of Chemistry, University of California, Irvine, California 92697-2025.

[3]Stanford Synchrotron Radiation Lightsource, SLAC National Accelerator Laboratory, Stanford University, Menlo Park, CA 94025

[4]Department of Chemistry, Stanford University, Stanford, CA 94305

Abstract

Nitrogenase is a versatile metalloenzyme that reduces N_2, CO and CO_2 at its cofactor site. Designated the M-cluster, this complex cofactor has a composition of [(*R*-homocitrate)$MoFe_7S_9C$], and it is assembled through the generation of a unique [Fe_8S_9C] core prior to the insertion of Mo and homocitrate. NifB catalyzes the crucial step of radical SAM-dependent carbide insertion concomitant with the coupling and rearrangement of two [Fe_4S_4] clusters into a [Fe_8S_8C] intermediate, as well as the subsequent incorporation of a '9^{th} sulfur' that completes the stoichiometry of the [Fe_8S_9C] core. This review focuses on the recent work that sheds light on the role of NifB in the formation of the [Fe_8S_9C] core of the nitrogenase cofactor, highlighting the structure, function and mechanism of this unique radical SAM methyltransferase.

Prologue

The intertwined relationship between the chemical and biological understanding of metallo-catalysts is beautifully depicted by Professor Richard H. (Dick) Holm in his comment from 2003: '*Traditionally, synthetic inorganic chemistry has provided the molecular intuition needed to interpret metal behavior in biological systems. Today, in a reversal of circumstance, metallobiomolecules are posing fundamental inorganic questions whose answers lie outside our existing knowledge. It is a fitting symmetry that the relationship between inorganic chemistry and biology has come full circle*' [1]. A remarkable case in point is the biological and chemical thrusts into the synthesis of the complex metallocofactor of nitrogenase or its synthetic mimics, which have drawn inspiration from each other over the past decades and converged recently on a semi-synthetic approach that combined a synthetic [Fe_4S_4] compound and a biological

*Corresponding author: Yilin Hu (yilinh@uci.edu); Markus W. Ribbe (mribbe@uci.edu), Britt Hedman (bhedman@stanford.edu), Keith O. Hodgson (hodgsonk@stanford.edu).

‖These authors contributed equally to this work.

Declaration of Competing Interests

The authors declare no competing financial and non-financial interests.

assembly platform, NifB, for the generation of an 8Fe core of the nitrogenase cofactor via radical SAM chemistry [2]. Motivated by Dick's seminal work on the chemical synthesis of nitrogenase cofactor mimics, this work demonstrated an effective use of Fe_4S_4 modules—both by Nature and in synthetic chemistry—as building blocks for the synthesis of high-nuclearity metallocofactors. Such a principle, most suitable to be featured in this special feature, was aptly described by Dick in 2016 as follows: '*Clusters containing the cubane-type Fe_4S_4 core play a central role in (cluster) conversion chemistry. The core conversion concept tends to reinforce the description of iron–sulfur cores as modular units subject to various covalent bond interactions that lead to different structures*' [3]. Equally fitting for this special feature, the water soluble synthetic [Fe_4S_4] compound used in conjunction with NifB was generated after Dick's pioneering work in this research area [4,5]. This review provides a concise summary of the current understanding of nitrogenase cofactor biosynthesis, with a particular emphasis on the cofactor core formation on NifB via fusion and rearrangement of [Fe_4S_4] modules—a topic in metalloprotein biochemistry that is strongly influenced and inspired by Dick Holm's seminal work in synthetic structural and functional bioinorganic chemistry.

Graphical Abstract

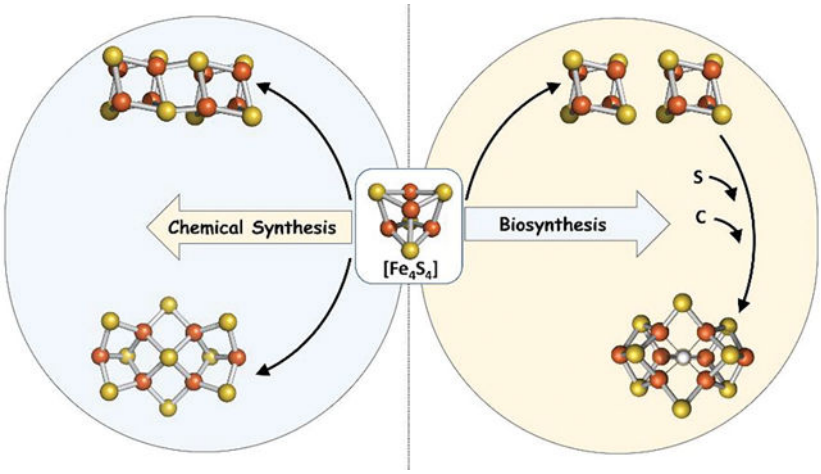

Fe_4S_4 modules are used as universal building blocks in synthetic chemistry and biological systems for the synthesis of high-nuclearity metallocenters, as illustrated by the biosynthesis of an 8Fe core of the nitrogenase cofactor (right) that mirrors the chemical synthesis of the 8Fe mimics of this cofactor core (left).

Keywords

nitrogenase; biosynthesis; FeS cluster; M-cluster; NifB; radical SAM enzyme

1. Introduction

The complex metalloenzyme nitrogenase catalyzes a variety of reductive reactions. Importantly, nitrogenase reduces atmospheric dinitrogen (N_2) to ammonia (NH_3) in the following reaction: $N_2 + 8H^+ + 16MgATP + 8e^- \rightarrow 2NH_3 + H_2 + 16MgADP + 16P_i$

[6–8]. In addition to dinitrogen, carbon monoxide (CO) can also be reduced by nitrogenase to short-chain hydrocarbons [9–11]. Interestingly, these two chemical transformations by nitrogenase mirror the industrial Haber-Bosch (HB) and Fischer-Tropsch (FT) processes, two important processes for large-scale nitrogen fertilizer and carbon fuel production, respectively [12–14]. However, there are clear distinctions between the nitrogenase reactions and their industrial counterparts. Most notably, while the industrial HB and FT processes use electrons supplied by hydrogen (H_2) gas as the reducing equivalents and require high temperatures and pressures to operate effectively, the nitrogenase-catalyzed HB- and FT-like reactions use protons and electrons as the substitute for H_2 and occur under ambient conditions. The less intensive parameters required by nitrogenase to undergo biological nitrogen fixation as compared to industrial processes make nitrogenase an ideal candidate for potential innovations in chemical energy. In particular, mechanistic insights into the biosynthesis and catalysis of nitrogenase could enable future development of biomimetic catalysts that harness the HB- and FT-type chemistry under mild conditions.

Our current knowledge of nitrogenase is mostly derived from the molybdenum (Mo)-dependent form of this enzyme, which consists of two protein components. One of these proteins, the Fe protein (or NifH), comprises two γ-subunits that each carry a MgATP binding site and jointly bridge a [Fe_4S_4] cluster at the subunit interface; the other protein, the MoFe protein (or NifDK), is a heterotetramer of $\alpha_2\beta_2$ composition that contains an M-cluster (also known as FeMoco or cofactor; [(*R*-homocitrate)$MoFe_7S_9C$]) within each α-subunit and a P-cluster ([Fe_8S_7]) at each α/β-subunit interface [15,16]. During catalysis, NifH and NifDK form a complex with each other, which permits interprotein electron transfer from the [Fe_4S_4] cluster on NifH to the metalloclusters on NifDK in an ATP-dependent process (Fig. 1) [6–8,17]. In this electron transfer model, the P-cluster first donates electrons to the M-cluster, on which substrate reduction occurs, and is subsequently refilled with electrons supplied from NifH. Other than N_2 and CO, nitrogenase can also reduce a number of substrates, such as carbon dioxide (CO_2), acetylene (C_2H_2), hydrazine (N_2H_4), nitrous oxide (N_2O) and azide (N_3^-), at ambient conditions, highlighting the catalytic versatility of the active-site M-cluster of this important mealloenzyme.

Possessing a uniquely complex composition for a metallocofactor, the M-cluster consists of [$MoFe_3S_3$] and [Fe_4S_3] subclusters that are connected to each other through an interstitial μ_6-carbide (C^{4-}) ion and three μ_2-sulfide (S^{2-}) atoms, with an additional homocitrate moiety coordinating its Mo-end [15,16]. Ligated by only two amino acids of NifDK—a Cys and a His—at its Fe- and Mo-end, respectively, the M-cluster can be extracted intact into an organic solvent, *N*-methylformamide (NMF) [18], and subsequently inserted into an inactive, cofactor-deficient form of NifDK [19] to restore enzymatic activity, illustrating the indispensable role of this metallocofactor in the catalytic function of nitrogenase [9,20,21].

Substantial progress has been made toward understanding the catalytic mechanism of nitrogenase, especially with regards to reductive events that occur at the active-site M-cluster. The most prominent mechanistic proposal concerning the M-cluster is the Lowe-Thorneley model [22–25]. Updated over the years [26,27], this model depicts the successive delivery of protons and electrons within the NifDK protein to the M-cluster for the binding, activation and reduction of substrate. Additionally, structural investigations of

inhibitor-bound nitrogenase have contributed significantly to our understanding of substrate activation, with a high-resolution crystal structure of Mo-nitrogenase revealing binding of a CO ligand to the M-cluster via displacement of a belt-sulfur atom (S2B) [28] and thereby suggesting a reaction mechanism involving generation of a reactive Fe species upon belt-sulfur displacement. A follow-up study using crystallographic pulse-chase methods with a Se-reporter further demonstrated the labile nature of the belt-sulfur atom S2B during catalysis [29] and the importance of a dynamic belt-sulfur region during substrate turnover. Recently, a crystal structure of NifDK with N_2 bound at the active site M-cluster revealed distinct dinitrogen species in the two M-clusters in place of the belt-sulfurs of NifDK [30], an unexpected observation that led to the proposal of a stepwise mechanism involving asynchronous rotations of the M-clusters in NifDK [30]. The structural assignment of belt sulfur displacement with N_2 was contested based on the modeling of N_2 and S—ligands indistinguishable at a resolution of 1.83 Å—at the belt sites [31], but this argument was refuted by the reproducibility of the sulfur anomalous data as well as a direct correlation between sulfur displacement (or replenishment) and N_2 release (or the lack thereof) [32]. While an improvement of the resolution of the crystal structure, along with further biochemical and spectroscopic evidence in support of the structural observation, is required to settle this debate, a recent DFT study led to the proposal of the removal of a belt sulfur as a prerequisite for N_2 binding [33], thereby lending additional support to the emerging theme of belt sulfur displacement by substrates during nitrogenase catalysis [28–30].

Alongside the studies of the catalytic mechanism of nitrogenase, considerable efforts have gone into the investigation of how the M-cluster is assembled. Understanding the detailed biosynthetic processes of the M-cluster can shed important lights on the structural-functional relationship of nitrogenase and facilitate the development of synthetic models that mimic the functions of nitrogenase. The current model of M-cluster biosynthesis involves three major assembly platforms (Fig. 2): (*i*) NifU, which interacts with NifS to mobilize iron (Fe) and sulfur (S) atoms for the generation of small [Fe_4S_4] units; (*ii*) NifB, which houses the coupling and rearrangement of two [Fe_4S_4] units into a [Fe_8S_9C] core concomitant with the insertion of an interstitial carbide and an additional sulfur atom; and (*iii*) NifEN, where the [Fe_8S_9C] core is matured into an M-cluster upon replacement of a terminal iron atom by Mo and homocitrate via the action of NifH [9,20,21]. Of all events that occur during the process of M-cluster assembly, those hosted by NifB are particularly interesting as this is the site where the unique core of the M-cluster, a motif with no parallel in the biological or synthetic realms, is generated. This review will provide a brief overview of the current understanding of M-cluster biosynthesis, followed by a detailed discussion of work that sheds light on the role of NifB in this process, highlighting the insertion of an interstitial carbide via radical SAM chemistry and the incorporation of a '9^{th} sulfur' into the catalytically labile, belt-sulfur region of the cofactor.

2. Biosynthesis of the M-cluster

Intermediates of the M-cluster biosynthetic pathway were identified by deleting certain nitrogen fixation (*nif*) genes [9,20,21]. These intermediates were captured on a variety of *nif*-encoded (Nif) proteins, including NifS/NifU, NifB, NifEN and NifDK. Various

biochemical, EPR, XAS/EXAFS and crystallographic studies [34–44] revealed sequential formation of the 2Fe-, 4Fe- and 8Fe-clusters on NifS/U and NifB. Substitution of Mo for one terminal Fe of the 8Fe-cluster and incorporation of homocitrate, mediated by NifH, leads to the formation of a mature M-cluster on NifEN, which can then be transferred to its binding site in NifDK (Fig. 2).

2.1. Generation of 4Fe Units on NifS/U

The assembly of the small 2Fe and 4Fe building blocks is achieved through the concerted actions of NifS and NifU. NifS, a pyridoxal phosphate-dependent cysteine desulfurase, catalyzes the formation of a protein-bound cysteine persulfide that is then donated to the assembly scaffold NifU for the synthesis and coupling of $[Fe_2S_2]$ fragments into $[Fe_4S_4]$ clusters (Fig. 2, ①) [34,35,45,46]. Subsequently, a $[Fe_4S_4]$ cluster pair is transferred to the next biosynthetic protein, NifB, where the two 4Fe clusters are fused into an 8Fe core of the M-cluster (Fig. 2, ②). EPR analysis has confirmed the $[Fe_4S_4]$ nature of the cluster species on NifB, showing an $S = 1/2$ signal in the dithionite-reduced protein that is characteristic of the $[Fe_4S_4]^{+}$ cluster. While the events that occur at the initial stage of cofactor assembly on NifS/U are rather straightforward from the perspective of the starting cluster species on NifB, the assembly protein immediately ‘downstream’ of NifS/U, details of the reactions catalyzed by NifS/U are yet to be fully elucidated.

2.2. Formation of an 8Fe Core on NifB

The formation of an 8Fe core of the cofactor occurs on NifB, a radical *S*-adenosyl-L-methionine (SAM) enzyme. Receiving a ‘transient’ $[Fe_4S_4]$ cluster pair (designated K-cluster) from NifU, NifB utilizes the radical SAM chemistry at its ‘permanent’ $[Fe_4S_4]$ cluster (designated SAM-cluster or radical SAM cluster) to couple the $[Fe_4S_4]$ cluster pair concomitant with insertion of a μ_6-coordinated interstitial carbide and a μ_2-coordinated belt-sulfide. Such actions of NifB result in the formation of a $[Fe_8S_9C]$ cluster (designated L-cluster) that is nearly indistinguishable from the mature M-cluster except for the substitution of one of the terminal Fe atoms for Mo/homocitrate (Fig. 2, ②) [36–40]. EPR analyses illustrated the K→L cluster conversion on NifB, showing the disappearance of the K-cluster specific, $S = 1/2$ signal in the dithionite-reduced state concomitant with the appearance of the L-cluster specific, $g = 1.92$ signal in the oxidized state [36]. XAS/EXAFS, XES and crystallographic studies provided further structural evidence for the formation of an L-cluster ($[Fe_8S_9C]$) before Mo and homocitrate are inserted that matures this cluster into an M-cluster [(*R*-homocitrate)$MoFe_7S_9C$]) (Fig. 2, ②) [37–40]. Most importantly, the insertion of a SAM-derived interstitial carbide that accompanies the coupling and rearrangement of the two 4Fe modules of K-cluster, along with the incorporation of a sulfite (SO_3^{2-})-derived ‘9^{th} sulfur’ that completes the stoichiometry of an 8Fe L-cluster, represent the unique chemistry that is employed for the biosynthesis of the nitrogenase cofactor (*see* 3 below for detailed discussion).

2.3. Maturation of the 8Fe Core on NifEN

Upon completion on NifB, the L-cluster is transferred to NifEN and matured into an M-cluster via incorporation of Mo and homocitrate by NifH in an ATP- and reductant-dependent process (Fig. 2, ③). Highly homologous to NifDK in the primary sequence and

tertiary structure, NifEN has four of the six cysteine ligands that coordinate the P-cluster in NifDK, accommodating a 'simpler' [Fe_4S_4] cluster instead of the [Fe_8S_7] P-cluster; in addition, it contains a region that approximates the active site of NifDK, preserving one M-cluster ligand with a Cys residue and replacing the other His ligand by an Asn residue. The substantial homology between NifEN and NifDK has led to the proposal that NifEN is involved in cofactor biosynthesis. Consistent with this proposal, an L-cluster-bound form of NifEN (designated $NifEN^L$) was captured [41] and examined by Fe K-edge XAS/EXAFS and crystallographic analyses, which revealed a nearly indistinguishable core structure of this cluster from that of the M-cluster [38,39]. Incubation of $NifEN^L$ with dithionite, NifH, MgATP, molybdate (MoO_4^{2-}) and homocitrate led to an M-cluster-bound form of NifEN (designated $NifEN^M$), pointing to a previously unknown function of NifH —the reductase component of Mo-nitrogenase—as an ATP- and reductant-dependent Mo/homocitrate insertase that is required for cofactor maturation [41,44]. It should be noted that NifQ, a non-essential *nif* gene product, was proposed to function as a Mo donor for cofactor maturation on NifEN/NifH complex [47,48]. However, the effects of *nifQ* deletion on the growth of free-living diazotrophic organisms, such as *Azotobacter vinelandii* and *Klebsiella pneumoniae*, could be effectively suppressed by addition of cystine or elevated concentrations of MoO_4^{2-} [49,50]. This observation, along with the dispensability of NifQ in many legume species [51], points to a possible 'housekeeping' role of NifQ, such as that in Mo/S storage, instead of a direct participation of this protein in the incorporation of Mo into the cofactor.

The L→M cluster conversion on NifEN was illustrated by the appearance of an $S = 3/2$ EPR signal in $NifEN^M$ that resembled the $S = 3/2$ signal of the M-cluster in NifDK, and the similarity between the Fe K-edge XAS/EXAFS features of $NifEN^M$ and NifDK [44]. Additionally, the M-cluster extracted from $NifEN^M$ displayed EPR and XAS/EXAFS characteristics indistinguishable from those of the M-cluster extracted from NifDK, further demonstrating that the M-cluster is fully assembled on NifEN prior to its transfer to NifDK [44,52].

2.4. Transfer of the mature M-cluster to NifDK

Following the L→M cluster conversion, the M-cluster is transferred from NifEN to its target binding site in NifDK (Fig. 2, ④). Comparative Fe chelation analyses of the cluster species in $NifEN^L$ and $NifEN^M$ suggested a conformational change of NifEN upon maturation of the L-cluster into an M-cluster, which rendered the nascent M-cluster 'buried' in a less solvent-accessible region of the α-subunit of this protein [52]. Biochemical experiments further demonstrated the capacity of NifEN to complex with apo NifDK only after the L→M cluster conversion, pointing to a crucial role of cluster maturation on NifEN in signaling the subsequent delivery of the M-cluster from NifEN to NifDK [9,20,21]. Transfer of the M-cluster between these two structurally homologous proteins is likely facilitated by the preservation of only one of the two M-cluster ligands of NifDK in NifEN. Additionally, several residues that presumably 'lock' the M-cluster in place at the active site of NifDK, including His^{442} and Trp^{444}, are absent from NifEN, permitting an easier release of the M-cluster from NifEN [53]. Consistent with this proposal, introduction of the 'lock' residues of NifDK into the corresponding positions in NifEN renders the latter incapable of releasing

the matured M-cluster to NifDK, an event that occurs under normal circumstances upon cluster maturation on NifEN [53]. Once released, the M-cluster likely travels from its binding site within the α-subunit of NifEN to the surface of the protein, where it is relayed to the surface of NifDK via coordinated actions of a pair of surface-located cysteinyl ligands —one Cys each from NifEN and NifDK— prior to being inserted into its target binding site along a positively charged 'cofactor insertion funnel' within the α-subunit of NifDK [19, 37].

3. Role of NifB as a radical SAM 'cofactor assemblase'

NifB plays a pivotal role in the formation of the unique 8Fe core of the cofactor. A radical *S*-adenosyl-L-methionine (SAM) enzyme, NifB is highly conserved across organisms harboring the nitrogenase enzyme. The essential role of NifB in nitrogenase cofactor assembly was illustrated by the expression of a cofactor-deficient, apo form of NifDK in *nifB*-deletion strains of *Azotobacter vinelandii* that rendered these strains incapable of nitrogen fixation [9,19–21]. Yet, how NifB carries out its function in the cofactor assembly process had remained elusive until recently, when structural and functional characterizations of several NifB species provided some much-needed clues to the mechanism of this unique radical SAM enzyme.

3.1. Structure and function of NifB

The first insights into the structural-functional relationship of NifB came from the sequence analysis of this protein. NifB carries a N-terminal CX_3CX_2C motif, a feature shared by other radical SAM enzymes, as well as a number of conserved cysteine and histidine residues that could potentially coordinate the Fe atoms of the M-cluster [54]. Consistent with the sequence-based prediction, the initial biochemical and CW EPR studies have revealed the presence of multiple $[Fe_4S_4]$ clusters on NifB that collectively give rise to a composite $S = 1/2$ EPR signal in the dithionite-reduced state [36,54,55]. The observation that apo NifB could be reconstituted with synthetic $[Fe_4S_4]$ clusters further confirmed the presence of $[Fe_4S_4]$ clusters in this protein [2]. Systematic mutagenesis of potential Cys ligands further identified three distinct $[Fe_4S_4]$ clusters in NifB, each showing a characteristic $S = 1/2$ EPR signal of the $[Fe_4S_4]^+$ cluster in the dithionite-reduced state [56]. One of these clusters, designated the SAM-cluster or radical SAM (RS) cluster, binds to the canonical SAM motif; whereas the other two, designated the K1- and K2-cluster, respectively, are a pair of proximal $[Fe_4S_4]$-like clusters comprising a so-called K-cluster. Other than the Cys ligands assigned to the RS-, K1- and K2-clusters, CW and pulse EPR spectroscopies also identified an additional, His-derived nitrogen ligand for the K1-cluster [56–58].

Crystallographic analyses of NifB proteins from methanogenic organisms provided further insights into the overall architecture of this protein, as well as the location and coordination of its associated $[Fe_4S_4]$ clusters [59,60]. The x-ray crystal structure of the FeS-reconstituted, holo NifB from *Methanobacterium thermoautotrophicum* (designated *Mt*NifB) reveals that the 'core' of this protein consists of a partial TIM barrel structure, a feature shared by several radical SAM enzymes [59–66]; additionally, there are three $[Fe_4S_4]$ clusters [59] located in the flexible regions of the protein within a space that is

'sectioned off' by the partial TIM barrel (Fig. 3a). Interestingly, combined crystallographic analyses and DFT calculations suggest that all clusters in the holo *Mt*NifB protein have a three-ligand coordination pattern, with three Cys ligands ligating the RS-cluster (Fig. 3b), and one His and two Cys ligands ligating each of the K1- and K2-clusters (Fig. 3c). Moreover, a SAM molecule can be modeled between the RS- and K1/K2-clusters, poised to interact with the differentiated '4^{th} Fe' site of one or more of these clusters to enable cluster conversion (Fig. 3d). Such an 'open' coordination pattern of all three clusters on NifB, coupled with the structural flexibility of the regions harboring these clusters, could facilitate a 'crosstalk' between the clusters and accommodate the dynamic biosynthetic events that occur on NifB.

Indeed, following incubation with SAM, the K-cluster-specific, $S = 1/2$ signal in the EPR spectrum of the dithionite-reduced NifB disappeared concomitant with the appearance of an L-cluster-specific, $g = 1.92$ signal in the EPR spectrum of the IDS-oxidized NifB [36,41,43,55]. It is important to note that the K-cluster displays a composite $S = 1/2$ EPR signal with all features of the $S = 1/2$ signals of the individual RS-, K1- and K2-clusters prior to treatment with SAM [56] and that a major change in the EPR characteristics only occurs upon interaction of the K-cluster with SAM and its subsequent conversion to an L-cluster [36,41,43,55]. These observations strongly refute a recent re-refinement of the same 3.0 Å dataset collected on *Mt*NifB that led to the proposal of a sequential incorporation of the K1- and K2-clusters, followed by a fusion of these two 4Fe clusters into an 8Fe cluster in the absence of SAM [67]. Such a proposal invokes a spontaneous coupling and rearrangement of the K1- and K2-clusters into a fully assembled P-cluster 'core', an unlikely—if not impossible—scenario given the highly involved and site-specific nature of P-cluster biosynthesis [20,21]. Curiously, the two 4Fe subcubanes of the hypothesized P-cluster 'core' are not only ligated by a μ_2-sulfide, but also edge-bridged by another μ_2-sulfide and a Cys-derived sulfur atom, rendering it somewhat analogous in architecture to a carbide-free L-cluster [67]. The absence of any P- or L-cluster related EPR signal from the SAM-untreated, K-cluster-bound NifB calls into question the existence of such a complex, fused 8Fe cluster with characteristics of both P- and L-clusters, and the scarcity of 'free' Fe sites in this hypothetical, high-nuclearity cluster species for the subsequent interaction with SAM contradicts the biochemical and spectroscopic observations of such interactions and the ensuing, radical SAM based cluster coupling and rearrangement, thereby casting serious doubt on the proposed spontaneous mechanism of cofactor formation. Clearly, while the 3.0 Å holo *Mt*NifB structure provides a crucial first look into the cluster species, ligand environment and reaction mechanism of NifB, a detailed molecular depiction of this enzyme requires high-resolution crystal structures of NifB before and after treatment with SAM and, perhaps equally importantly, biochemical and spectroscopic data that align with the structural data, which could minimize any potential ambiguity and overinterpretation of the structural data.

The fact that the highly complex K→L cluster conversion can be accomplished by a 'simple' treatment of NifB with SAM points to a novel radical SAM-dependent synthetic route to a bridged, high-nuclearity metallocofactor [9,20,54]. Yet, how NifB couples and rearranges two $[Fe_4S_4]$ clusters into a $[Fe_8S_9C]$ core alongside the incorporation of an

interstitial carbide and a '9th sulfur' entails some unique chemistry that has no parallel in other biological systems.

3.2. Mechanistic insights into the 8Fe core formation on NifB

Recently, a combination of biochemical, spectroscopic and structural studies, assisted by the successful expression of NifB from various organisms in *E. coli*, have defined the function of NifB as a radical SAM methyltransferase that hosts a multitude of biosynthetic events during the formation of an 8Fe core of the nitrogenase cofactor; in particular, the insertion of an interstitial carbide that plays a central role in generating a '9th sulfur' deplete 8Fe core, followed by insertion of a sulfite-derived '9th sulfur' in the belt region of the 8Fe core, highlights the intricacy of the mechanism utilized by NifB for the biosynthesis of a functional nitrogenase cofactor.

3.2.1. Insertion of an interstitial carbide—The origin and insertion of the interstitial carbide were first probed by high-performance liquid chromatography–mass spectrometry (HPLC-MS), which allowed for the identification of products resulting from incubation of NifB with SAM. Treatment of NifB with unlabeled SAM resulted in the formation of *S*-adenosyl-homocysteine (SAH) and 5'-deoxyadenosine (5'-dAH) as the SAM cleavage products [55,68,69]; whereas treatment of NifB with methyl-d_3-SAM resulted in SAH and a mixture of monodeuterated 5'-dAD and 5'-dAH [68]. The identities of these cleavage products suggest that two events occurred upon interaction of NifB with SAM. One of them involves donation of a methyl group from one equivalent of SAM to the substrate, producing SAH as a byproduct; whereas the other involves homolytic cleavage of a second equivalent of SAM, resulting in a highly reactive 5'-adenosyl radical (5'-dA•) species that subsequently abstracts a hydrogen atom from the methyl group to yield 5'-dAH. Radiolabeling experiments revealed that incubation of NifB with [methyl-^{14}C]-SAM resulted in an accumulation of the ^{14}C label in NifB, and the ^{14}C label could be further traced to the L-cluster extracted from NifB [55,68]. These experiments further demonstrated a transfer of the ^{14}C-labeled L-cluster from NifB to NifEN, where it was matured into a ^{14}C-labeled M-cluster prior to insertion into its binding site in NifDK [55,68]. Together, these observations strongly suggest that the interstitial carbide is derived from the methyl group of SAM, which undergoes hydrogen atom abstraction by a 5'-dA• radical before it is further processed into a carbide ion and incorporated into the center of an L-cluster.

The observation that the ^{14}C label was incorporated into the L-cluster instead of being retained by the polypeptides of NifB [68] suggests that the methyl group is directly transferred from SAM onto the substrate (in this case, the K-cluster) without being routed through a protein-bound carbon intermediate. In support of this suggestion, treatment of NifB unlabeled and [methyl-d_3] SAM, respectively, generated methanethiol (CH_3SH) and methane-d_3-thiol (CD_3SH) as the products of these reactions [68], suggesting a transfer of the SAM-derived methyl group to an acid-labile S atom of the K-cluster as the first step of carbide insertion [68,69]. Additionally, substitution of the [Fe_4S_4] clusters on NifB with [Fe_4Se_4] clusters resulted in the formation of methylselenol (CH_3SeH) upon acid quenching, providing further evidence for the cluster-associated S atom as the initial site for the attachment of the SAM-derived methyl group [69]. These results collectively point to the

transfer of the SAM-derived methyl group to an acid labile S atom of the K-cluster via an S_N2-type reaction.

To further delineate the sequence of events between methyltransfer and hydrogen abstraction, NifB was incubated with allyl-SAM, a SAM analog wherein the methyl group is replaced by an allyl (CH_2=CH–CH_2–) moiety. HPLC-MS analysis revealed SAH as the sole product of SAM cleavage in this reaction; whereas GC-MS analysis indicated release of allylthiol (CH_2=CH–CH_2–SH) upon acid quenching of the reaction mixture [69]. Such an observation can only be explained by allylation of an acid labile S atom of the K-cluster by the first allyl-SAM equivalent, followed by binding of a second allyl-SAM equivalent to the SAM-motif cluster that is unable to undergo homolytic cleavage to generate 5'-dA• for the subsequent hydrogen atom abstraction. By analogy, methylation of the K-cluster must precede the radical-mediated steps that convert the methyl group into an interstitial carbide. Such a process is somewhat analogous to the initial methylation step in the process of C–C bond formation by Cfr and RlnM, two important radical SAM enzymes involved in RNA methylation [70]. However, unlike Cfr and RlnM, NifB does not employ a Cys residue for the methyltransfer, and this event only occurs in the presence of a reductant [69]. The latter observation is particularly interesting, as it suggests the necessity to poise the K-cluster at a certain redox potential to render the cluster S atom sufficiently nucleophilic for methyltransfer through an S_N2-type mechanism.

Combined mutagenic, biochemical, spectroscopic and crystallographic studies led to further insights into the methyltransfer and hydrogen atom abstraction events that occur during the early stage of carbide insertion (Fig. 4a, ①–③). HPLC-MS and GC-MS analyses of NifB variants carrying single cluster modules (*i.e.*, the RS-, K1- or K2-cluster) or double cluster modules (*i.e.*, RS+K1, RS+K2) established that K2- and RS-clusters are required for the formation of SAH/5'-dAH and CH_3SH, respectively, as the product(s) of SAM cleavage and acid quenching [56]. This observation allows for an assignment of the functions of the K2- and RS-clusters, with the K2-cluster receiving a methyl group from SAM upon interaction of SAM with the RS-cluster (Fig. 4a, ②), followed by hydrogen atom abstraction from the K2-bound methyl group that gives rise to a methyl-derived radical species (Fig. 4a, ③). With respect to the K1-cluster, pulse EPR spectroscopy led to the identification of a histidine-derived nitrogen ligand for this cluster module (Fig. 4a, ①) [56,57]. Identified as His^{43} of NifB from *Methanosarcina acetivorans* (designated *Ma*NifB), this conserved histidine ligand was not detected by pulse EPR following the treatment of NifB with SAM, during which process the K1- and K2-clusters are coupled and rearranged into an L-cluster on NifB [56,57]. Mutation of His^{43} to Ala in *Ma*NifB did not impact the SAM cleavage profile; however, it resulted in the inability of this *Ma*NifB variant to generate an L-cluster upon incubation with SAM and dithionite [57]. XAS/EXAFS analysis of SAM-treated *Ma*NifB H43A suggested formation of a cluster intermediate comprising two 4Fe subclusters, with a carbon that has not fully transitioned into its completely deprotonated carbide form and that is either attached to one or both K-cluster modules (Fig. 4b) [57]. Given the presence of an imidazole ring in histidine that is capable of proton delivery, the His^{43} ligand of *Ma*NifB could serve dual functions in the K→L-cluster transformation, orienting the K1-cluster for proper coupling with the K2-cluster while also enabling deprotonation of the carbon radical species to promote carbide formation. Interestingly,

while crystallographic analyses of NifB from *M. thermoautotrophicum* (*Mt*NifB) confirmed His^{31} (of *Mt*NifB) as the equivalent of His^{43} (of *Ma*NifB) as the nitrogen ligand for the K1-cluster, DFT calculations suggested His^{24} of this protein as another potential nitrogen ligand for the K2-cluster in *Mt*NifB [59]. Like His^{31}, His^{24} may play a role in orienting the K2-cluster for its coupling with the K1-cluster while facilitating deprotonation of the initial carbon radical alongside His^{31} and, possibly, other conserved residues (*e.g,* His or Arg) in the areas surrounding the K1- and K2-clusters.

A mechanism can be proposed for carbide insertion (*see* Fig. 4a) based on these observations, which begins with an S_N2-type transfer of the methyl group from SAM to a K2-associated S atom. This event is followed by the formation of a putative methylene radical (*S*–CH_2•) via hydrogen atom abstraction from the transferred methyl group by 5'-dA•. The reactive *S*–CH_2• species, which is attached to the K2-cluster, then binds to an Fe atom of the K1-cluster to initiate cluster fusion and rearrangement while undergoing deprotonation and ligand exchange itself until a μ_6-coordinated carbide is embedded in the center of an L-cluster. It is plausible that deprotonation of the SAM-derived methylene intermediate is coupled with protonation of the His ligands of the K1- and K2-clusters, and that the loss of these ligands upon protonation not only facilitates cluster coupling and rearrangement, but also labilizes the newly formed L-cluster to allow its transfer from NifB to the next biosynthetic apparatus, NifEN.

3.2.2. Insertion of a '9th sulfur'—The stoichiometry of the L-cluster is completed by addition of a '9th S' atom, an event that accompanies the fusion and reorganization of the K1- and K2-clusters concomitant with insertion of an interstitial carbide. Probing the origin and fate of the '9th S' has long been hindered by the introduction of unwanted sulfide aggregates that result from traditional $FeCl_3/Na_2S$-based cluster reconstitution methods. Recently, a new FeS reconstitution method was developed, which involved reconstitution of *Ma*NifB with a water-soluble, synthetic $[Fe_4S_4]$ compound ($[Fe_4S_4(SCH_2CH_2OH)_4]^{2-}$; designated $[Fe_4S_4]^{Syn}$) [4,5] in order to prevent formation of sulfide aggregates. Subsequently, the reconstituted *Ma*NifB protein was incubated with SAM and one of the three physiological sulfur sources, sulfide (S^{2-}), sulfite (SO_3^{2-}) or sulfate (SO_4^{2-}), in the presence of a sulfur-free reductant, Eu^{II}-EGTA ($E^{0\prime}$ = −0.8 V at pH 8) and examined for the K→L cluster conversion under these conditions [2,71]. These experiments revealed that maturation of a K-cluster to an L-cluster on *Ma*NifB only occurred in the presence of SO_3^{2-} [2]. Consistent with this observation, substitution of unlabeled SO_3^{2-} with $^{35}SO_3^{2-}$ in the same incubation mixture led to accumulation of the ^{35}S radiolabel on *Ma*NifB, which could be further traced to the L-cluster isolated from this protein [2]. Together, these results firmly established SO_3^{2-} as a source of the '9th S' for cofactor biosynthesis.

Interestingly, HPLC profiles and EPR analyses revealed that *Ma*NifB treated with SAM has identical SAM cleavage products and EPR features in the presence or absence of SO_3^{2-} [2]. However, only the SO_3^{2-}-treated *Ma*NifB was capable of donating an L-cluster to NifEN that could be further matured into an M-cluster prior to its transfer to NifDK [2,72]. The observation that the SAM-treated *Ma*NifB displayed the same, 8Fe-core-specific, g = 1.94 signal in the presence or absence of SO_3^{2-} is particularly intriguing, as it implies that the radical SAM-dependent carbide insertion and the concurrent 8Fe-core rearrangement (Fig.

5, ①–③) occur prior to the insertion of the 9th S atom. These results led to the proposal of a new [Fe_8S_8C] intermediate, termed the L*-cluster, which closely resembles the [Fe_8S_9C] L-cluster in architecture but lacks a '9th S' that is present in the belt region of the L-cluster (Fig. 5, ④).

CW/Pulse EPR, XAS/EXAFS and MCD studies were then performed to probe the identity and architecture of the proposed L*-cluster [73,74]. 3p-ESEEM experiments revealed that, treatment of *Ma*NifB with SAM in the absence of SO_3^{2-} (yielding the L*-cluster), like that in the presence of SO_3^{2-} (yielding the L-cluster), resulted in a loss of nitrogen (*i.e.*, the histidine ligand) coupling to the cluster [73]. This result suggests that a structural rearrangement of the protein scaffold that involves a 'loss' of the histidine ligand to the cluster species has already occurred upon the K→L* cluster conversion [73]. In agreement with this observation, the *Ma*NifB proteins treated with SAM in the absence and presence of SO_3^{2-} displayed the same pre-edge XAS feature corresponding to the unusual geometry of the 8Fe-core [73]. XAS/EXAFS analyses further pointed to a structural similarity between the L*- and L-clusters despite some differences indicating a less constrained conformation of the L*-cluster due to the missing belt sulfur [73]. The absence of a μ_2-coordinated belt sulfide from the L*-cluster is consistent with the labile nature of the belt region of the cofactor [28–30], which facilitates activation of the Fe sites coordinated by the belt sulfide(s) upon their displacement during catalysis. Interestingly, MCD and EPR analyses revealed identical structures of the *Ma*NifB-associated L*- and L-clusters upon oxidation [73], suggesting movement of the belt sulfide away from the oxidized L-cluster that somewhat mirrors the belt sulfide displacement of the M-cluster upon turnover [28–30].

Taken together, these studies not only identified the source of the '9th S', but also clarified the sequence of events between carbide insertion and '9th S' incorporation (Fig. 5). The pathway depicting the formation of the 8Fe-core on NifB can be further refined based on these results, with carbide insertion occurring concurrently with the coupling and rearrangement of two [Fe_4S_4] clusters (*i.e.*, the K1- and K2-clusters) into a [Fe_8S_8C] cluster (or the L*-cluster), followed by insertion of SO_3^{2-} as the '9th S^{2-}' that completes the architecture of a [Fe_8S_9C] cofactor core (or the L-cluster) (Fig. 5). It is important to note that while the vacant belt sulfur site of the L*-cluster is presumably filled by a nearby cysteine thiolate or water ligand, it can be easily refilled upon incubation with sulfite. Such a feature could prove instrumental in labeling the catalytically important belt region of the M-cluster to enable future mechanistic investigations of nitrogenase.

3.3. Relationship of NifB with other radical SAM enzymes

A large number of proteins that are highly homologous to NifB have been identified through BLAST. This family of proteins can be divided into two groups—full-length and truncated—depending on whether the NifX domain, a sequence that is non-essential for nitrogenase cofactor assembly [54,55], is present in their sequences (Fig. 6). Proteobacteria, such as *Azotobacter vinelandii*, have full-length NifB proteins; whereas a variety of other microbes, such as euryarcheotes and firmicutes, have truncated NifB proteins [54,55]. Notably, while some hosts of the truncated NifB proteins (*e.g.*, *M. thermoautotrophicus* and *M. acetivorans*) are nitrogen-fixing organisms [54,55], other members of this group (*e.g.*, *M.*

thermoacetophila) do not carry nitrogenase-encoding genes [75]. This observation points to a functional diversity of the NifB protein family that is consistent with the wide range of functionality of the radical SAM enzyme family.

A comparison of *Mt*NifB (Fig. 7a) with other radical SAM enzymes (Fig. 7b–g) reveals that although these enzymes share a common structural core that consists of a partial TIM barrel, much of their structural diversity arises from variations in their accessory components, including auxiliary domains and clusters. The pyruvate formate-lyase activating enzyme (PFLae), which lacks accessory components, is perhaps one of the 'simplest' radical SAM enzymes that shares considerable structural homology with *Mt*NifB (Fig. 7b) [76]. Lipoyl synthase (LipA) and MoaA, on the other hand, each carry one auxiliary [Fe_4S_4] cluster that, like the K1- or K2-cluster in *Mt*NifB, has an open Fe site to enable sulfur donation in the case of LipA or substrate activation in the case of MoaA. However, contrary to the centrally located K1- and K2-clusters in *Mt*NifB, the auxiliary clusters in LipA and MoaA are located at the extensions of the core structure (Fig. 7c, d) [77,78]. The structural similarity and distinction are also apparent with *Mt*NifB is compared with the anaerobic sulfatase maturating enzyme (anSME) and peptide-modifying enzyme SuiB (Fig. 7e, f), two additional members of the radical SAM enzyme family [79,80]. Like *Mt*NifB, both anSME and SuiB carry an RS-cluster and two auxiliary clusters; however, while the K1- and K2-clusters of *Mt*NifB are each ligated by three residues of the protein, the auxiliary clusters of anSME and SuiB are fully coordinated and situated within the SPASM domain, which is distinct from the radical SAM core.

As far as the function of NifB in cofactor assembly is concerned, perhaps the best analog to this enzyme is RlmN, a radical SAM methyltransferase involved in the methylation of ribosomal RNA (Fig. 7g) [81]. RlmN and NifB share the same mode-of-action in their respective functions, catalyzing methyltransfer from the first equivalent of SAM and hydrogen atom abstraction from the methyl group by a 5'-dA• radical derived from the second equivalent of SAM. However, while the methyl group is transferred to a Cys residue (Cys^{355}) by RlmN prior to its incorporation into the substrate through an S_N2 mechanism, the methyl group is transferred onto a K2-cluster-associated sulfide by NifB through an S_N2-like mechanism. Both reaction mechanisms of RlmN and NifB then proceed with hydrogen atom abstraction from the SAM-derived methyl group, resulting in a methylene radical that either enables the methylation of adenosine 2503 (by RlmN) or initiates the process of carbide insertion concomitant with cluster fusion and reorganization (by NifB). A structural overlay of holo *Mt*NifB with SAM-bound RlmN reveals that the methylated Cys^{355} residue occupies the space between the SAM molecule in RlmN and the K2-cluster in *Mt*NifB (Fig. 8). Moreover, the conserved Cys^{118} residue of RlmN, which likely facilitates the abstraction and subsequent donation of a proton for the methylation of the adenosine 2503, is located near the His^{31} residue of *Mt*NifB, which is presumably involved in the deprotonation of the methylene radical species (Fig. 8). Despite a clear distinction in their identities and the reactions they catalyze, the Cys^{355} and K2-sulfide, which initially receive the SAM-derived methyl group, and the Cys^{118} and His^{31}, which are involved in proton abstraction, demonstrate analogous roles and positioning in RlmN and *Mt*NifB, showcasing a certain similarity in the mechanisms of these distinct radical SAM enzymes.

The common traits shared between NifB and RlmN place NifB in the broad category of radical SAM methyltransferases (RSMTs) [54,55], a subset of radical SAM enzymes that catalyze methyltransfer using SAM or other methyl-containing donors. However, NifB clearly does not belong to the previously defined classes B, C and D of RSMTs, which carry additional domains other than the canonical radical SAM (RS) domain [64,65,82]. Thus, NifB can be tentatively categorized as a member of a new class of RSMTs that consist of an RS domain and two FeS cluster-binding domains [64,65,82]. Although NifB shares a certain mode-of-action with class A RSMTs (*e.g.*, RlmN and Cfr), it does not have a pair of conserved Cys residues (*e.g.*, Cys^{335}/Cys^{118} of RlmN) that are usually found in the sequences of class A RSMTs, including one that serves as the site of intermediary methylation. Consequently, NifB is unable to conduct methyltransfer via a protein residue [64,65,82]; instead, it catalyzes a direct transfer of the methyl group from SAM to the FeS cluster(s) that are coordinated by conserved Cys and His residues flanking the RS domain, with the methyl group undergoing subsequent radical SAM-dependent transformations to assist the assembly of a complex metallocluster [54,55].

4. Conclusions

NifB plays a pivotal role in the maturation of the nitrogenase cofactor, catalyzing the radical SAM-dependent incorporation of an interstitial carbide and a '9^{th} sulfur' concomitant with the coupling and rearrangement of two [Fe_4S_4] clusters into an [Fe_8S_9C] core that is nearly indistinguishable from, and hence easily convertible into, a mature M-cluster with a composition of [(*R*-homocitrate)$MoFe_7S_9C$]. Recent structural, spectroscopic, and biochemical studies have provided a better understanding of the structure, function and mechanism of NifB; whereas classification of a family of NifB proteins as a distinct subset of radical SAM methyltransferases not only points to a broader range of functions carried out by these proteins, but also opens up new avenues for investigations into this relatively uncharacterized, yet chemically unique enzyme family.

Acknowledgments

The authors were supported by NIH-NIGMS grants GM67626 (to MWR and YH) and GM141046 (to YH and MWR), which funded research related to nitrogenase assembly and catalysis, respectively. KH and BH acknowledge support from NIH-NIGMS grants P41GM103393 and P30GM133894 as well as funding from the DOE Office of Biological and Environmental Research for the SSRL Structural Molecular Biology Program that enabled the x-ray spectroscopy work referenced herein.

Abbreviations:

Fe protein	iron protein
MoFe protein	molybdenum-iron protein
M-cluster	iron-molybdenum cofactor
SAM	*S*-adenosylmethionine
SAH	*S*-adenosylhomocysteine
5'-dAH	5'-deoxyadenosine

XAS	x-ray absorption spectroscopy
EXAFS	extended x-ray absorption fine structure
EPR	electron paramagnetic resonance
CW	continuous wave
ESEEM	electron spin echo envelop modulation
MCD	magnetic circular dichroism
DFT	density functional theory

References

[1]. Lee SC, Holm RH, Proc. Natl. Acad. Sci. USA 100 (2003) 3595–600. [PubMed: 12642670]

[2]. Tanifuji K, Lee CC, Sickerman NS, Tatsumi K, Ohki Y, Hu Y, Ribbe MW, Nat. Chem. 10 (2018) 568–572. [PubMed: 29662207]

[3]. Holm RH, Lo W, Chem. Rev. 116 (2016) 13685–13713. [PubMed: 27933770]

[4]. Averill BA, Herskovitz T, Holm RH, Ibers JA, J. Am. Chem. Soc. 95 (1973), 3523–3534. [PubMed: 4708377]

[5]. Barclay JE, Davies SC, Evans DJ, Hughes DL, Inorg. Chim. Acta 291 (1999) 101–108.

[6]. Burgess BK, Lowe DJ, Chem. Rev. 96 (1996) 2983–3012. [PubMed: 11848849]

[7]. Buscagan TM, Rees DC, Joule 3 (2019) 2662–2678. [PubMed: 32864580]

[8]. Rutledge HL, Tezcan FA, F. A. Chem. Rev. 120 (2020) 5158–5193.

[9]. Jasniewski AJ, Lee CC, Ribbe MW, Hu Y, Chem. Rev. 120 (2020) 5107–5157. [PubMed: 32129988]

[10]. Hu Y, Lee CC, Ribbe MW, M. W. Science 333 (2011) 753–755.

[11]. Lee CC, Hu Y, Ribbe MW, Science 329 (2010) 642. [PubMed: 20689010]

[12]. Emsley J, Nature 410 (6829) 633–634.

[13]. Schlö R, Angew. Chem., Int. Ed. 42 (2003) 2004–2008.

[14]. Rofer-DePoorter CK, Chem. Rev. 81 (1981) 447–474.

[15]. Lancaster KM, Roemelt M, Ettenhuber P, Hu Y, Ribbe MW, Neese F, Bergmann U, DeBeer S Science 334 (2011) 974–977. [PubMed: 22096198]

[16]. Spatzal T, Aksoyoglu M, Zhang L, Andrade SL, Schleicher E, Weber S, Rees DC, Einsle O, O. Science 334 (2011) 940.

[17]. Schindelin H, Kisker C, Schlessman JL, Howard JB, Rees DC, Nature 387 (1997) 370–376. [PubMed: 9163420]

[18]. Shah VK, Brill WJ Proc. Natl. Acad. Sci. USA 74 (1977), 3249–3253. [PubMed: 410019]

[19]. Schmid B, Ribbe MW, Einsle O, Yoshida M, Thomas LM, Dean DR, Rees DC, Burgess BK, Science 296 (2002), 352–356. [PubMed: 11951047]

[20]. Ribbe MW, Hu Y, Hodgson KO, Hedman B, Chem. Rev. 114 (2014) 4063–4080. [PubMed: 24328215]

[21]. Ribbe MW, Hu Y, Annu. Rev. Biochem. 85 (2016) 455–483. [PubMed: 26844394]

[22]. Lowe DJ, Thorneley RNF, Biochem. J. 224 (1984) 877–886. [PubMed: 6395861]

[23]. Lowe DJ, Thorneley RNF, Biochem. J. 224 (1984) 895–901. [PubMed: 6395863]

[24]. Thorneley RNF, Lowe DJ, Biochem. J. 224 (1984) 887–894. [PubMed: 6395862]

[25]. Thorneley RNF, Lowe DJ, Biochem. J. 224 (1984) 903–909. [PubMed: 6395864]

[26]. Hoffman BM, Lukoyanov D, Yang ZY, Dean DR, Seefeldt LC, Chem. Rev. 114 (2014) 4041–4062. [PubMed: 24467365]

[27]. Rohde M, Sippel D, Trncik C, Andrade SLA, Einsle O, O. Biochemistry 57 (2018), 5497–5504.

[28]. Spatzal T, Perez KA, Einsle O, Howard JB, Rees DC, Science 345 (2014) 1620–1623. [PubMed: 25258081]

[29]. Spatzal T, Perez KA, Howard JB, Rees DC, Elife 4 (2015) e11620. [PubMed: 26673079]

[30]. Kang W, Lee CC, Jasniewski AJ, Ribbe MW, Hu Y, Science 368 (2020) 1381–1385. [PubMed: 32554596]

[31]. Peters JW, Einsle O, Dean DR, DeBeer S, Hoffman BM, Holland PL, Seefeldt LC, Science 371 (2021) eabe5481. [PubMed: 33574183]

[32]. Kang W, Lee CC, Jasniewski AJ, Ribbe MW, Hu Y, Science 371 (2021) eabe5856. [PubMed: 33574184]

[33]. Wei WJ, Siegbahn PEM, Chemistry (2022) e202103745. [PubMed: 35098591]

[34]. Yuvaniyama P, Agar JN, Cash VL, Johnson MK, Dean DR, Proc. Natl. Acad. Sci. USA 97 (2000) 599–604. [PubMed: 10639125]

[35]. Zheng LM, Dean DR, J. Biol. Chem. 269 (1994) 18723–18726. [PubMed: 8034623]

[36]. Wiig JA, Hu Y, Ribbe MW, Proc. Natl. Acad. Sci. USA 108 (2011) 8623–8627. [PubMed: 21551100]

[37]. Kaiser JT, Hu Y, Wiig JA, Rees DC, Ribbe MW, Science 331 (2011) 91–94. [PubMed: 21212358]

[38]. Fay AW, Blank MA, Lee CC, Hu Y, Hodgson KO, Hedman B, Ribbe MW, Angew. Chem. Int. Ed. Engl. 50 (2011) 7787–7790. [PubMed: 21726031]

[39]. Corbett MC, Hu Y, Fay AW, Ribbe MW, Hedman B, Hodgson KO, Proc. Natl. Acad. Sci. USA 103 (2006) 1238–1243. [PubMed: 16423898]

[40]. Lancaster KM, Hu Y, Bergmann U, Ribbe MW, Debeer S, J. Am. Chem. Soc. 136 (2013) 610–612. [PubMed: 24367925]

[41]. Hu Y, Fay AW, Ribbe MW, Proc. Natl. Acad. Sci. USA, 102 (2005) 3236–3241. [PubMed: 15728375]

[42]. Hu Y, Corbett MC, Fay AW, Webber JA, Hodgson KO, Hedman B, Ribbe MW, Proc. Natl. Acad. Sci. USA 103 (2006) 17125–17130. [PubMed: 17062756]

[43]. Hu Y, Corbett MC, Fay AW, Webber JA, Hodgson KO, Hedman B, Ribbe MW, Proc. Natl. Acad. Sci. USA 103 (2006) 17119–17124. [PubMed: 17050696]

[44]. Yoshizawa JM, Blank MA, Fay AW, Lee CC, Wiig JA, Hu Y, Hodgson KO, Hedman B, Ribbe MW, J. Am. Chem. Soc. 131 (2009) 9321–9325. [PubMed: 19514721]

[45]. Zheng L, White RH, Cash VL, Jack RF, Dean DR, Proc. Natl. Acad. Sci. USA 90 (1993) 2754–2758. [PubMed: 8464885]

[46]. Smith AD, Jameson GNL, Dos Santos PC, Agar JN, Naik S, Krebs C, Frazzon J, Dean DR, Huynh BH, Johnson MK, Biochemistry 44 (2005) 12955–12969. [PubMed: 16185064]

[47]. Hernandez JA, Curatti L, Aznar CP, Perova Z, Britt RD, Rubio LM, Proc. Natl. Acad. Sci. USA 105 (2008) 11679–116884. [PubMed: 18697927]

[48]. George SJ, Hernandez JA, Jimenez-Vicente E, Echavarri-Erasun C, Rubio LM, Chem. Commun. (Camb) 79 (2016) 11811–11814.

[49]. Rodríguez-Quiñones F, Bosch R, Imperial J, J. Bacteriol. 175 (1993) 2926–2935. [PubMed: 8491713]

[50]. Ugalde RA, Imperial J, Shah VK, Brill WJ, J. Bacteriol. 164 (1985) 1081–1087. [PubMed: 3905765]

[51]. Saad MM, Michalet S, Fossou R, Putnik-Delić M, Crèvecoeur M, Meyer J, de Malézieux C, Hopfgartner G, Maksimović I, Perret X X, Mol. Plant Microbe Interact. 32 (2019) 208–216. [PubMed: 30070615]

[52]. Fay AW, Blank MA, Rebelein JG, Lee CC, Ribbe MW, Hedman B, Hodgson KO, Hu Y, Proc. Natl. Acad. Sci. USA 113 (2016) 9504–9508. [PubMed: 27506795]

[53]. Solomon JB, Lee CC, Jasniewski AJ, Rasekh MF, Ribbe MW, Hu Y, Angew. Chem. Int. Ed. Engl. 59 (2020) 6887–6893. [PubMed: 32022452]

[54]. Hu Y, Ribbe MW, Curr. Opin. Chem. Biol. 31 (2016) 188–194. [PubMed: 26969410]

[55]. Fay AW, Wiig JA, Lee CC, Hu Y, Proc. Natl. Acad. Sci. USA 112 (2015) 14829–14833. [PubMed: 26627238]

[56]. Rettberg LA, Wilcoxen J, Lee CC, Stiebritz MT, Tanifuji K, Britt RD, Hu Y, Nat. Commun. 9 (2018) 2824. [PubMed: 30026506]

[57]. Rettberg LA, Wilcoxen J, Jasniewski AJ, Lee CC, Tanifuji K, Hu Y, Britt RD, Ribbe MW, Nat. Commun. 11 (2020) 1757. [PubMed: 32273505]

[58]. Wilcoxen J, Arragain S, Scandurra AA, Jimenez-Vicente E, Echavarri-Erasun C, Pollmann S, Britt RD, Rubio LM, J. Am. Chem. Soc. 138 (2016) 7468–7471. [PubMed: 27268267]

[59]. Kang W, Rettberg LA, Stiebritz M, Jasniewski AJ, Tanifuji K, Lee CC, Ribbe MW, Hu Y, Angew. Chem. Int. Ed. Engl, 60 (2021) 2364–2370. [PubMed: 33035363]

[60]. Fajardo AS, Legrand P, Payá-Tormo LA, Martin L, Pellicer Martı Nez MT, Echavarri-Erasun C, Vernède X, Rubio LM, Nicolet Y, J. Am. Chem. Soc. 142 (2020) 11006–11012. [PubMed: 32476412]

[61]. Frey PA, Hegeman AD, Ruzicka FJ, Crit. Rev. Biochem. Mol. Biol. 43 (2008) 63–88. [PubMed: 18307109]

[62]. Broderick JB, Duffus BR, Duschene KS, Shepard EM, Chem. Rev. 114 (2014) 4229–4317. [PubMed: 24476342]

[63]. Vey JL, Drennan CL, Chem. Rev. 111 (2011) 2487–2506. [PubMed: 21370834]

[64]. Mulliez E, Duarte V, Arragain S, Fontecave M, Atta M M Front. Chem. 5 (2017) 17. [PubMed: 28361051]

[65]. Lanz ND, Booker SJ, Biochim. Biophys. Acta. 1853 (2015) 1316–1334. [PubMed: 25597998]

[66]. Banerjee R, J. Biol. Chem. 290 (2015) 3962–3963. [PubMed: 25477525]

[67]. Jenner LP, Cherrier MV, Amara P, Rubio LM, Nicolet Y, Chem Sci. 12 (2021) 5269–5274. [PubMed: 34168778]

[68]. Wiig JA, Hu Y, Lee CC, Ribbe MW, Science 337 (2012) 1672–1675. [PubMed: 23019652]

[69]. Wiig JA, Hu Y, Ribbe MW, Nat. Commun. 6 (2015) 8034. [PubMed: 26259825]

[70]. Bauerle MR, Schwalm EL, Booker SJ, J. Biol. Chem. 290 (2015) 3995–4002. [PubMed: 25477520]

[71]. Vincent KA, Tilley GJ, Quammie NC, Streeter I, Burgess BK, Cheesman MR, Armstrong FA, Chem. Commun. (Camb) 20 (2003) 2590–2591.

[72]. Tanifuji K, Jasniewski AJ, Villarreal D, Stiebritz MT, Lee CC, Wilcoxen J, Okhi Y, Chatterjee R, Bogacz I, Yano J, Kern J, Hedman B, Hodgson HO, Britt RD, Hu Y, Ribbe MW, Nat Chem. 2021 Oct 11. doi: 10.1038/s41557-021-00799-8. Online ahead of print.

[73]. Jasniewski AJ, Wilcoxen J, Tanifuji K, Hedman B, Hodgson KO, Britt RD, Hu Y, Ribbe MW, Angew. Chem. Int. Ed. Engl. 58 (2019) 14703–1470. [PubMed: 31411369]

[74]. Rupnik K, Tanifuji K, Rettberg LA, Ribbe MW, Hu Y, Hales B, Chembiochem 21 (2020) 1767–1772. [PubMed: 31881119]

[75]. The nifD and nifK genes that encode the subunits of nitrogenase, characterized by the presence of distinct P- and M-cluster ligands, are absent from the genome of M. *thermoacetophila* based on BLAST search performed at https://img.jgi.doe.gov/.

[76]. Vey JL, Yang J, Li M, Broderick WE, Broderick JB, Drennan CL, Proc. Natl. Acad. Sci. USA 105 (2008) 16137–16141. [PubMed: 18852451]

[77]. McLaughlin MI, Lanz ND, Goldman PJ, Lee K-H, Booker SJ, Drennan CL, Proc. Natl. Acad. Sci. USA 113 (2016) 9446–9450. [PubMed: 27506792]

[78]. Hänzelmann P, Schindelin H, Proc. Natl. Acad. Sci. USA 101 (2004) 12870–12875. [PubMed: 15317939]

[79]. Davis KM, Schramma KR, Hansen WA, Bacik JP, Khare SD, Seyedsayamdost MR, Ando N, Proc. Natl. Acad. Sci. USA 114 (2017) 10420–10425. [PubMed: 28893989]

[80]. Goldman PJ, Grove TL, Sites LA, McLaughlin MI, Booker SJ, Drennan CL, Proc. Natl. Acad. Sci. USA 110 (2013) 8519–8524. [PubMed: 23650368]

[81]. Boal AK, Grove TL, McLaughlin MI, Yennawar NH, Booker SJ, Rosenzweig AC, Science 332 (2011) 1089–1092. [PubMed: 21527678]

[82]. Zhang Q, van der Donk WA, Liu W, Acc. Chem. Res. 45 (2012) 555–564. [PubMed: 22097883]

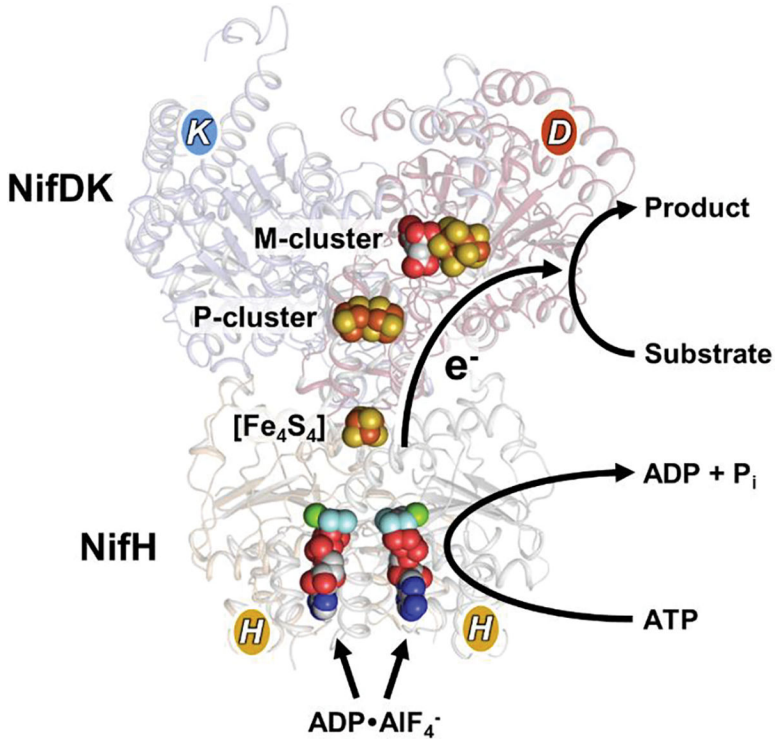

Fig. 1.

Crystal structure of half of the ADP•AlF_4^--stabilized NifH/NifDK complex of Mo-nitrogenase. NifH and NifDK are shown in ribbon presentations and rendered transparent, with the two subunits of NifH colored yellow and light brown, and the α ('D', NifD) and β ('K', NifK) subunits of NifDK colored red and blue, respectively. The $[Fe_4S_4]$ cluster, P-cluster ($[Fe_8S_7]$ M-cluster ([(*R*-homocitrate)$MoFe_7S_9C$]) and MgADP•AlF_4^- are shown in ball-and-stick presentations, with the atoms colored as follows: Fe, orange; S, yellow; Mo, cyan; O, red; C, gray; N, dark blue; Mg, green; Al, beige; F, light blue. PyMOL was used to generate this figure.

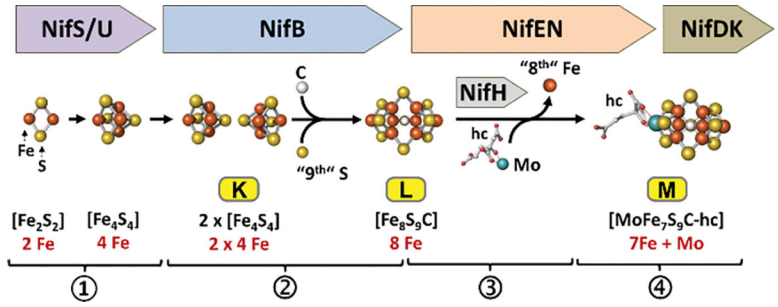

Fig. 2.

Assembly pathway of the M-cluster. The pathway begins with the combined actions of NifS and NifU, which catalyze the sequential formation of $[Fe_2S_2]$ and $[Fe_4S_4]$ clusters (①). Subsequently, a pair of $[Fe_4S_4]$ clusters (K-cluster) are delivered to NifB, where they are coupled into a $[Fe_8S_9C]$ (L-cluster) concomitant with insertion of an interstitial C and a "9^{th} S" (②). The L-cluster is then transferred to NifEN, where it is matured into an [(*R*-homocitrate)$MoFe_7S_9C$] (M-cluster) via NifH-mediated substitution of Mo and homocitrate (hc) for a terminal Fe (③). This event is followed by transfer of the M-cluster to its target location in NifDK, which completes the M-cluster assembly process (④). The clusters are shown in ball-and-stick presentations, with the atoms colored as follows: Fe, orange; S, yellow; Mo, cyan; O, red; C, gray. PyMOL was used to generate this figure.

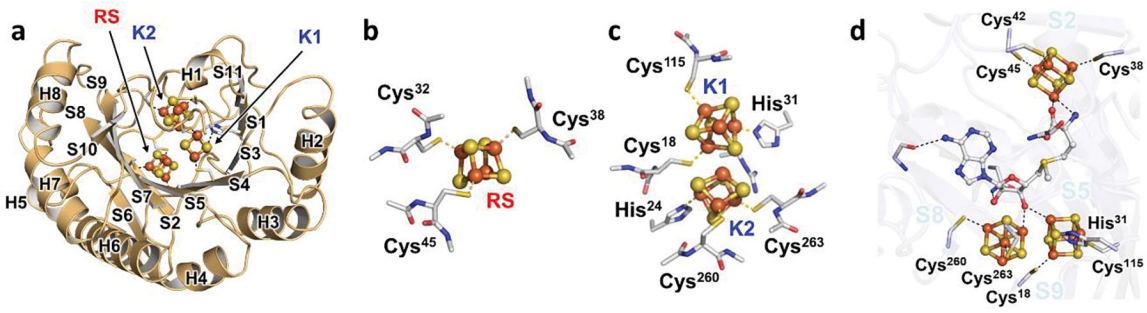

Fig. 3.

(**a**) Side view of the holo *Mt*NifB structure highlighting the TIM barrel core. (**b**, **c**) DFT-optimized (TPSS/def2-SVP) structure of the RS-cluster (b) and K1/K2-cluster pair (c) and their respective ligand environments in holo *Mt*NifB. The DFT calculations were carried out using a minimal atomic model. Based on EPR data, all clusters were assumed to be in the $[Fe_4S_4]^+$ state and, in the case of the K1/K2-cluster pair, an S=1 spin state was considered based on possible ferromagnetic coupling. The average Fe-S (2.35 Å) and Fe-Fe (2.75 Å) distances of the three $[Fe_4S_4]$ clusters in the DFT-optimized models are in strong agreement with results from the Fe K-edge XAS/EXAFS analysis of holo *Mt*NifB. (**d**) Model of holo *Mt*NifB with SAM bound between the RS-cluster and the K1/K2-modules. The peptides are shown in ribbon presentation; the clusters and SAM are shown in ball-and-stick presentations; and the coordinating ligands are shown as sticks. The atoms are colored as follows: Fe, orange; S, yellow; O, red; C, gray; N, dark blue. PyMOL was used to generate this figure.

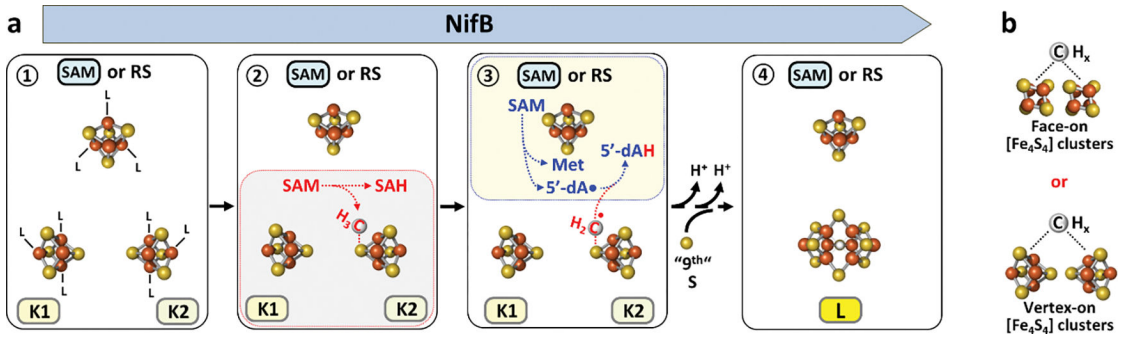

Fig. 4.

Insertion of the interstitial carbide. (**a**) Events that occur during carbide insertion on NifB. NifB contains three 3-ligand (labeled 'L', where L refers to a Cys or His ligand) coordinated $[Fe_4S_4]$ clusters: the SAM (or RS)-, K1- and K2-clusters (①). In the case of *Mt*NifB, crystallographic analyses and DFT calculations have led to the assignment of three Cys ligands for the SAM (or RS)-cluster and two Cys ligands and one His ligand for each of the K1- and K2-clusters. Cleavage of the first SAM molecule results in the formation of SAH and the transfer of a methyl group to an S atom of K2 via an S_N2-type mechanism (②). This event is followed by cleavage of the second SAM molecule, which results in the formation of a SAM-cluster-bound methionine (Met) and a 5′-dA• radical that abstracts a hydrogen atom from the K2-bound methyl group, generating an S atom-bound methylene radical (③). Continued deprotonation of the K2-bound methylene radical eventually gives rise to an interstitial carbide concomitant with the coupling and rearrangement of K1 and K2, and this event is followed by insertion of a "9^{th} S" in the belt region, leading to the formation of an 8Fe L-cluster (④). (**b**) Substitution of Ala for the His ligand of K1 results in a carbon intermediate (CH_x) bridged between K1 and K2, either face-on (upper) or vertex-on (lower), suggesting a role of the nitrogen ligand in deprotonating the carbon species derived from the initial methylene radical.

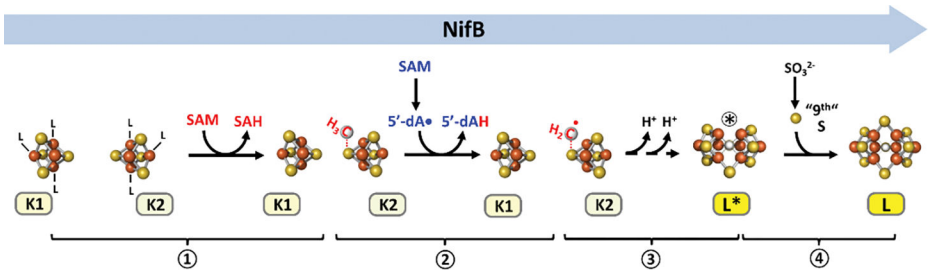

Fig. 5.

Insertion of the "9th S". Refined pathway of 8Fe core (L-cluster) formation on NifB, which involves transfer of a methyl group from one SAM equivalent to an S atom of K2 via an S_N2-type mechanism (①), followed by abstraction of a hydrogen atom from the K2-bound methyl group by a second SAM equivalent-derived 5′-dA• radical, generating a S atom-bound methylene radical (②). The methylene radical then initiates the rearrangement and coupling of K1 and K2 while undergoing continued deprotonation, leading to the formation of an L*-cluster ($[Fe_8S_8C]$) that has the interstitial carbide in place but lacks one belt sulfur (③). This event is followed by insertion of the "9th S" into the L*-cluster, which gives rise to an L-cluster ($[Fe_8S_9C]$) that closely resembles the metal-sulfur core of the mature M-cluster in structure (④).

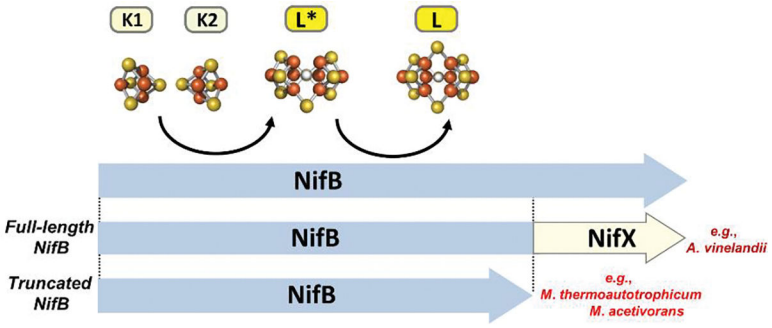

Fig. 6.

The NifB protein family. Phylogenetic analyses categorize the NifB protein family as ‘full-length’ and ‘truncated’ based on the presence or absence of the non-essential ‘NifX domain’ that is located near the C-terminus of the sequence.

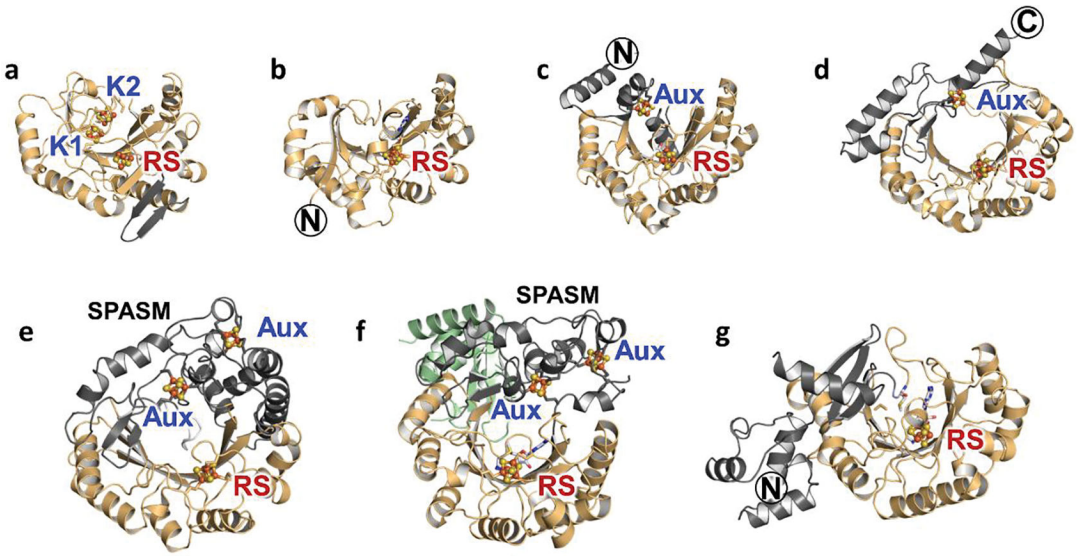

Fig. 7.

Structures of various radical SAM enzymes. Shown are the ribbon presentations of (**a**) holo *Mt*NifB (PDB ID: 7JMB), (**b**) formate-lyase activating enzyme (PDB ID: 3CB8), (**c**) lipoyl synthase (PDB ID: 5EXI), (**d**) MoaA (PDB ID: 1TV7), (**e**) anaerobic sulfatase maturating enzyme anSME (PDB ID: 4K39), (**f**) peptide-modifying enzyme SuiB (PDB ID: 5V1S), and (**g**) RlmN (PDB ID: 3RFA). The common, partial TIM barrel cores in these structures are shown in orange, and the additional, variable domains are shown in teal. The RS-, K1-, K2- and auxiliary (Aux) clusters are shown as ball-and-sticks, with Fe and S atoms colored orange and yellow, respectively. The SPASM domain, the name of which is derived from its involvement in the maturation of subtilosin A, pyrroloquinoline quinone, anaerobic sulfatase, and mycofactocin, is indicated. PyMOL was used to generate the figure.

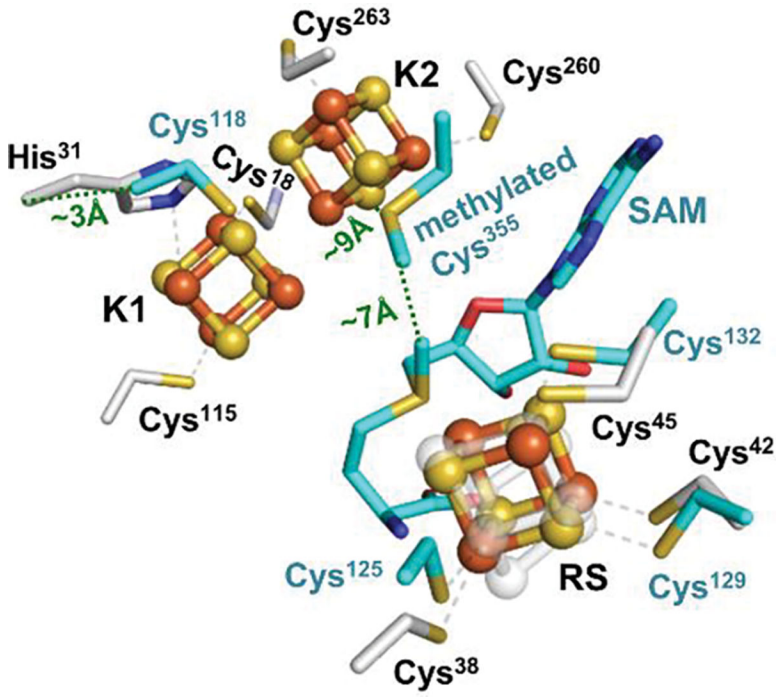

Fig. 8.

Structural overlay of holo *Mt*NifB and SAM-treated RlmN. The RS-, K1- and K2-clusters of *Mt*NifB are shown in ball-and-stick presentations, with Fe and S colored orange and yellow, respectively. The RS-cluster of RlmN is depicted the same way but rendered transparent. The ligands of the RS-, K1- and K2-clusters in *Mt*NifB are shown as sticks, with atoms colored as follows: S, yellow; C, gray; N, dark blue. The ligands of the RS-cluster, the catalytically important cysteines (Cys^{118} and the methylated Cys^{355}) and the bound SAM molecule in RlmN are depicted and colored the same way as those in *Mt*NifB, except that C is colored cyan. PyMOL was used to generate the figure.